

Complex patterns arise through spontaneous symmetry breaking in dense homogeneous networks of neural oscillators

Rajeev Singh, Shakti N. Menon and Sitabhra Sinha

The Institute of Mathematical Sciences, CIT Campus, Taramani, Chennai 600113, India.

(Dated: November 6, 2018)

Recent experiments have highlighted how collective dynamics in networks of brain regions affect behavior and cognitive function. In this paper we show that a simple, homogeneous system of densely connected oscillators representing the aggregate activity of local brain regions can exhibit a rich variety of dynamical patterns emerging via spontaneous breaking of permutation or translational symmetry. Our results connect recent experimental findings and suggest that a range of complicated activity patterns seen in the brain could be explained even without a full knowledge of its wiring diagram.

PACS numbers: 05.45.Xt, 89.75.Kd, 87.19.L-

Collective dynamics of coupled oscillators, in particular, synchronization [1], is integral to many natural phenomena [2] and is especially important for several biological processes [3], such as brain function [4, 5]. While very large-scale synchronization of neuronal activity is considered pathological, as in epilepsy [6], the brain is capable of exhibiting a variety of complex spatiotemporal excitation patterns that may play a crucial role in information processing [7]. Understanding the dynamics of these patterns at the scale of the entire brain (imaged using techniques such as fMRI) is of fundamental importance, as interaction between widely dispersed brain regions are responsible for significant behavioral changes, such as loss of consciousness caused by disruption of communication between different areas of the cerebral cortex [8]. As detailed simulation of each individual neuron in the brain is computationally expensive [9], when studying the dynamics of the entire system it is useful to focus on the network of interactions between brain regions. It has also been explicitly shown that the collective response of a large number of connected excitatory and inhibitory neurons, which constitute such regions, can be much simpler than the dynamics of individual neurons [10]. Indeed, each region can be described using phenomenological models in terms of a few aggregate variables [11].

Using anatomical and physiological data obtained over several decades, the networks of brain regions for different animals have been reconstructed [12, 13], where the individual nodes correspond to large assemblies ($10^3 - 10^6$) of neurons [14]. The connectivity C (i.e., fraction of realized links) of these networks ($C \sim 10^{-1}$) is significantly higher than that among neurons ($C \sim 10^{-6}$) [15]. A schematic representation of a network of the Macaque brain regions (adapted from Ref. [13]) is shown in Fig. 1 (a). The collective activity of such networks can result in complicated nodal dynamics, including temporal oscillations at several scales that are known to be functionally relevant [5, 17]. Each of these nodes can be described using neural field models of localized neuronal population ac-

tivity, which can have varying mathematical complexity and biological realism [18]. In this paper, we use the well-known and pioneering model proposed by Wilson and Cowan (WC) [19] to describe the activity of each brain region. The resulting temporal patterns of the nodes in the Macaque network shown in Fig. 1 (b) are reminiscent of experimentally recorded activity of brain regions [5].

The complex collective dynamics observed for the network at different connection strengths [Fig. 1 (c)-(d)] can arise from an interplay of several factors, which makes their analysis difficult. A possible approach to understand the genesis of these patterns is to focus on the dynamics of the nodes interacting in the simplified setting of a homogeneous, globally coupled system, which is an idealization of the densely connected network. In this paper we show that this simple system exhibits an unexpectedly rich variety of complex phenomena, despite lacking the detailed topological features of brain networks [e.g., Fig. 1 (a)], such as heterogeneity in degree (number of connections per node) and modular organization. In particular, we show the existence of novel collective states, including those characterized by oscillator clusters, where each cluster is distinguished by its amplitude or frequency. The occurrence of such clusters is surprising as each node is identical in terms of both intrinsic dynamics and connectivity, indicating that the homogeneous system of oscillators undergoes *spontaneous symmetry breaking*. In addition we observe patterns where the time-series for all oscillators are identical except for a non-zero phase difference between n_{cl} groups of exactly synchronized elements which we refer to as “phase clusters”. On removing a few links from the network while preserving the structural symmetry of connections we observe even more dramatic situations such as the appearance of many (> 2) clusters having different amplitudes. In addition, oscillator death, which is seen over a substantial region of parameter space in the fully connected system, occurs in a drastically reduced region for such marginally sparse networks. As the behavior of a large, densely connected system is effectively identical to that

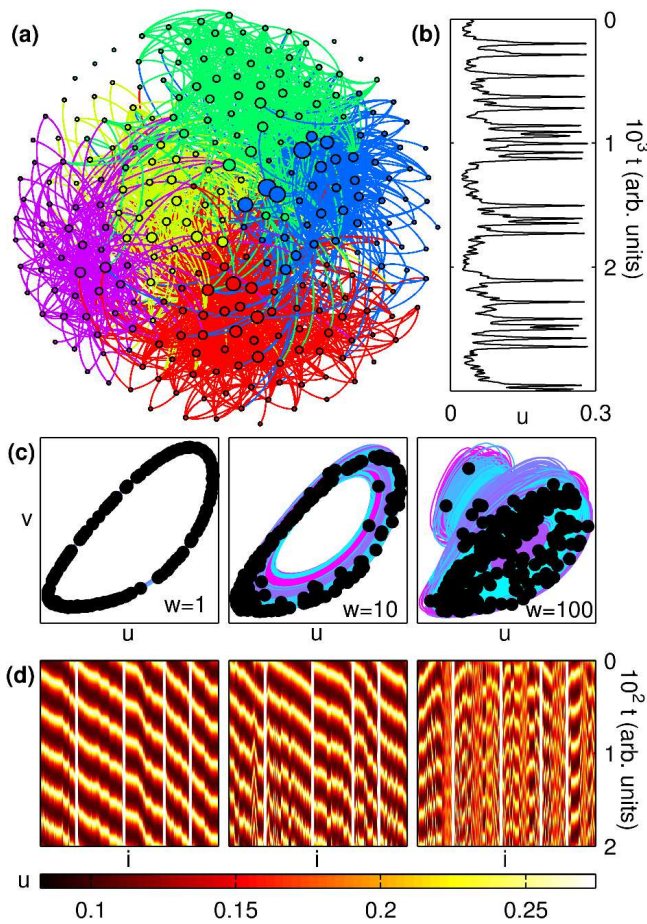


FIG. 1: (color online). (a) The directed network of connections between regions of the Macaque brain, adapted from Ref. [13]. The size of each node is proportional to its total degree and the colors distinguish the modules (characterized by significantly higher intra-connection density and obtained using a partitioning algorithm [16]). The color of each link corresponds to that of the source node. (b) Time series of the excitatory component of a typical node in this network with coupling strength $w = 500$, where each node is modeled as a Wilson-Cowan oscillator. (c) Phase space projections of the oscillators, obtained for different coupling strengths, where the filled circles represent the location of each oscillator at a time instant. The panels here are scaled individually for better visualization. (d) Time-series of the excitatory component u , for the corresponding values of w used in the panels directly above. The nodes i are arranged according to their modules (demarcated by white lines).

of the corresponding mean-field model, it is remarkable that the dynamical properties of the system considered here are radically altered in response to extremely minor deviations from the fully connected situation.

The model we consider comprises a network of N oscillators, each described by the WC model whose dynamics results from interactions between an excitatory and an inhibitory neuronal subpopulation. The average activity

of each node i (u_i, v_i) evolves as:

$$\begin{aligned}\tau_u \dot{u}_i &= -u_i + (\kappa_u - r_u u_i) \mathcal{S}_u(u_i^{in}), \\ \tau_v \dot{v}_i &= -v_i + (\kappa_v - r_v v_i) \mathcal{S}_v(v_i^{in}),\end{aligned}\quad (1)$$

where, $u_i^{in} = c_{uu}u_i - c_{uv}v_i + \sum' (w_{ij}^{uu}u_j - w_{ij}^{uv}v_j) + I_u^{ext}$ and $v_i^{in} = c_{vu}u_i - c_{vv}v_i + \sum' (w_{ij}^{vu}u_j - w_{ij}^{vv}v_j) + I_v^{ext}$ represent the total input to the two subpopulations respectively. The time constants and external stimuli for the subpopulations are indicated by $\tau_{u,v}$ and $I_{u,v}^{ext}$ respectively, while $c_{\mu\nu}$ ($\mu, \nu = u, v$) corresponds to the strength of interactions within and between the subpopulations of a node. The interaction strengths are represented by the weight matrices $W^{\mu\nu} = \{w_{ij}^{\mu\nu}\}$ and the summation \sum' is over all network neighbors. The function $\mathcal{S}_\mu(z) = [1 + \exp\{-a_\mu(z - \theta_\mu)\}]^{-1} + \kappa_\mu - 1$ has a sigmoidal dependence on z , with $\kappa_\mu = 1 - [1 + \exp(a_\mu\theta_\mu)]^{-1}$. The parameter values have been chosen such that each isolated node ($W^{\mu\nu} = 0$) is in the oscillatory regime, viz., $a_u = 1.3$, $\theta_u = 4$, $a_v = 2$, $\theta_v = 3.7$, $c_1 = 16$, $c_2 = 12$, $c_3 = 15$, $c_4 = 3$, $r_u = 1$, $r_v = 1$, $\tau_u = 8$, $\tau_v = 8$, $I_u^{ext} = 1.25$ and $I_v^{ext} = 0$. For the homogeneous systems considered here the links will have same strength, i.e., $w_{ij}^{\mu\nu} = w/k$ ($\mu, \nu = u, v$ and $i \neq j = 1, \dots, N$), where k is the degree of a node

The dynamical system (Eq. 1) is numerically solved using an adaptive-step Runge-Kutta integration scheme for different system sizes (N) and coupling strengths (w). Linear stability analysis is used to determine the stability of some of the patterns and identify the associated bifurcations. The behavior of the system for each set (w, N) is analyzed over many (~ 100) randomly chosen initial conditions. We have explicitly verified that our results are robust with respect to small variations in the parameters.

We first examine the collective dynamics of a pair of coupled oscillators ($N = 2$) as a function of the interaction strength between them. Fig. 2 (a)-(b) show that while exact synchronization (ES) of oscillator dynamics occurs at weak coupling ($w \lesssim 3.2$), a state of anti-phase synchronization (APS) is observed at higher values of w ($4.4 \lesssim w \lesssim 11$). For intermediate w , the co-existence of the dominant frequencies corresponding to ES and APS states [Fig. 2 (c)] indicates that the quasi-periodic behavior observed in this regime can be interpreted as arising through competition between the mechanisms responsible for the above two states. At $w \sim 11$, the system undergoes spontaneous symmetry-breaking, eventually giving rise to inhomogeneous in-phase synchronization (IIS), characterized by different phase-space projections and distinct amplitudes for the time-series of each oscillator [Fig. 2 (a)-(b), last panel]. The nature of the transition from APS to IIS is made explicit in Fig. 2 (d) [top panel], where the fixed points of one of the oscillators, obtained using numerical root finding, are shown over a range of w . At $w \approx 10.943$, a pair of hetero-

ogeneous unstable solutions related by permutation symmetry, corresponding to an inhomogeneous steady-state (ISS), emerge from a homogeneous unstable solution, beyond which all three solutions coexist. Thus, spontaneous symmetry breaking appears to arise in the system through a subcritical pitchfork bifurcation, with the number of positive eigenvalues corresponding to the homogeneous solution decreasing by unity (not shown). The ISS is stable over a very small range, $10.964 \lesssim w \lesssim 11.002$, as seen from their corresponding eigenvalues in Fig. 2 (d) [lower panel]. Note that stability is lost on either end of this interval through supercritical Hopf bifurcations. For $w \gtrsim 700$, both oscillators converge to the inactive state $u_i = v_i = 0, \forall i$, corresponding to amplitude death (AD, not shown).

Increasing the number of oscillators, we observe that while the patterns seen for a pair of coupled oscillators, namely ES, QP, ISS, IIS, APS and AD persist (first four shown in Fig. 3 (a)-(b) for $N = 20$) [20], qualitatively different states also emerge. As mentioned earlier, a new class of patterns characterized by the existence of phase clusters appears. The most robust of these, referred to as gradient synchronization (GS), has $n_{cl} \sim N$. Another new pattern comprises two oscillator clusters, each characterized by a unique frequency [Fig. 3 (c)]. This constitutes a dramatic instance of spontaneous breaking of permutation symmetry, as the oscillators are intrinsically indistinguishable for this completely homogeneous system. Thus, the appearance of multiple frequencies in a dynamical network need not imply heterogeneity in connectivity or node properties.

A third new pattern is a homogeneous steady state referred to as oscillator death (OD), in which the individual nodes have the same time-invariant, non-zero activity. This dynamical state appears over a large region in (w, N) -space as seen in the phase diagram, Fig. 3 (d). To identify and segregate the regimes in this diagram, we use several order parameters. The mean of the oscillation amplitude, measured as the variance (σ^2) with respect to time of one of the WC variables, v , averaged over all the nodes $\langle \sigma_i^2(v_i) \rangle_i$, is zero for all the non-oscillating states AD, OD and ISS. These are further distinguished by using the mean and variance with respect to all nodes of the time-averaged v , i.e., $\langle \langle v_i \rangle_t \rangle_i$ ($=0$ for AD) and $\sigma_i^2(\langle v_i \rangle_t)$ ($=0$ for OD and AD). To distinguish between the oscillating patterns, we consider the mean coherence, measured as $\langle \sigma_i^2(v_i) \rangle_t$, and the total space occupied by all the trajectory projections Δ , as measured by the number of non-zero bins of their histogram in (u, v) -space. ES is characterized by $\langle \sigma_i^2(v_i) \rangle_t = 0$ and IIS by $\sigma_i^2(\langle v_i \rangle_t) > 0$. The remaining patterns, GS and QP, are distinguished by $\Delta \sim 0$ for GS. Note that $\langle \rangle_t$ and $\langle \rangle_i$ represent averaging over time and all nodes, respectively. In practice, different regimes are characterized by thresholds whose specific values do not affect the qualitative nature of the results.

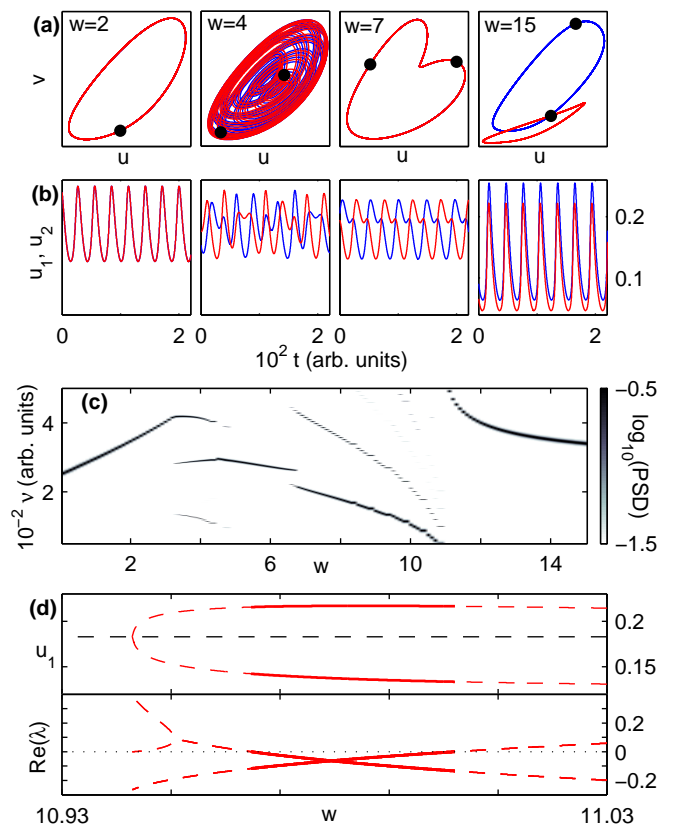


FIG. 2: (color online). Collective dynamics of a system of two coupled WC oscillators. (a) Phase space projections of the trajectories and (b) time-series for each oscillator showing exact synchronization (ES, for coupling $w = 2$), quasiperiodicity (QP, $w = 4$), anti-phase synchronization (APS, $w = 7$) and inhomogeneous in-phase synchronization (IIS, $w = 15$). The filled circles represent the location of each oscillator in phase space at a time instant. The panels in (a) are scaled individually for better visualization. (c) Power-spectral density (PSD) of the time-series for the u component of each oscillator, revealing the dominant frequencies as a function of w . (d) All fixed points of the system (upper panel) and the real parts of the eigenvalues corresponding to the heterogeneous fixed points (lower panel) showing the transitions between APS and IIS regimes. Solid (broken) lines represent stable (unstable) solutions.

As a first step towards extending the results seen for the globally coupled system to brain networks of the type shown in Fig. 1 (a), we have investigated the consequences of gradually decreasing the connection density. To ensure that the degree reduction preserves as many of the existing symmetries as possible, we arrange the nodes on a circle and sequentially remove connections between nodes placed furthest apart. In addition to preserving degree homogeneity, this ensures that every node has the same neighborhood structure. As we deviate from the global coupling limit, we observe patterns similar to those shown in Fig. 3 (a-d), although the precise form of

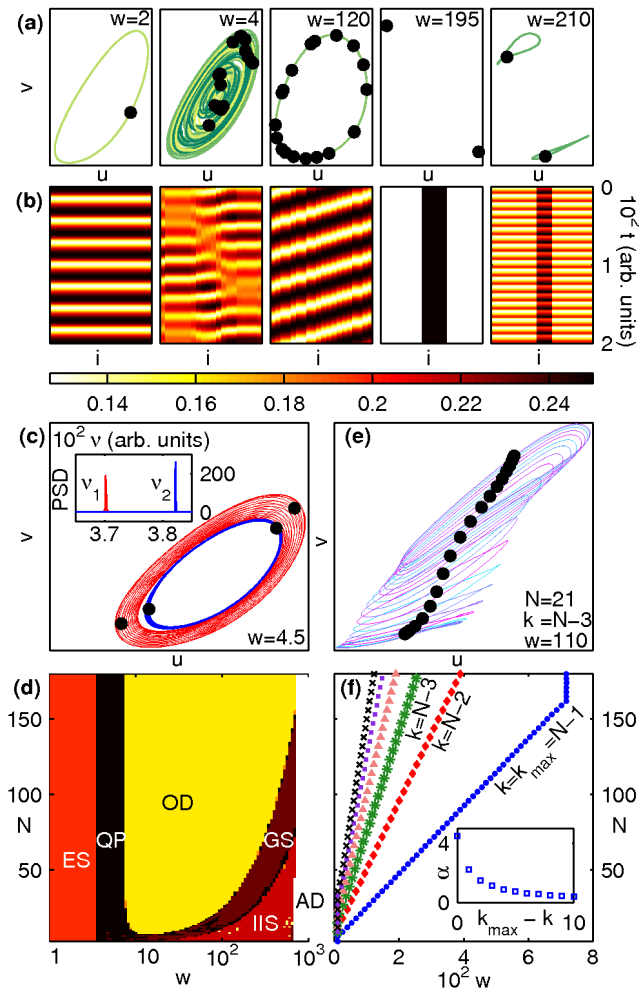


FIG. 3: (color online). Collective dynamics of N densely connected WC oscillators. (a) Phase space projections of the trajectories and (b) time-series for $N = 20$ globally coupled oscillators, showing exact synchronization (ES, $w = 2$), quasiperiodicity (QP, $w = 4$), gradient synchronization (GS, $w = 120$), inhomogeneous steady-state (ISS, $w = 195$) and inhomogeneous in-phase synchronization (IIS, $w = 210$). The panels in (a) are scaled individually for better visualization. (c) Phase space projections of the different oscillators for $w = 4.5$, which form two clusters with frequencies ν_1 and ν_2 , indicated by the power-spectral density (PSD, inset). (d) Phase diagram for N WC oscillators globally coupled with strength w , indicating areas where the majority ($> 50\%$) of initial conditions result in ES, QP, GS, IIS, oscillator death (OD) and amplitude death (AD). Note that the w -axis is logarithmic. (e) As the degree k , i.e., the number of links per node, deviates slightly from the globally coupled case ($k_{max} = N - 1$) to $N - 3$, the trajectories of the IIS state split into many ($\sim N$) distinct projections ($N = 21, w = 110$). (f) The OD region in (d) shrinks rapidly with the number of removed links, as seen from the slope of the upper boundary of OD (inset).

the attractors may differ and it is now the translational symmetry that is being spontaneously broken. For example, as seen in Fig. 3 (e), a reduction of just 2 links per node causes the trajectory in the IIS state to split into many more ($\sim N$) projections than seen for the fully connected case (~ 2). Also, while the phase diagram of the system remains qualitatively unchanged when the degree is decreased from $k_{max} = N - 1$, there is a dramatic quantitative reduction in the area corresponding to OD [Fig. 3 (f)] even with the reduction of one link per node. This is surprising, as one would expect that a marginal deviation from the global coupling limit in large systems will not result in a perceptible change from the mean-field behavior.

Our result that weakening connections between nodes of a network can increase coherence in collective activity (viz., observation of ES at low w) suggests an intriguing relation between two recent experimental findings: (i) anaesthetic-induced loss of consciousness occurs through the progressive disruption of communication between brain areas [8] and (ii) functional connectivity networks reconstructed from EEG data become increasingly dense with the development of fatigue in sleep-deprived subjects [21]. The latter study finds that the onset of sleep is accompanied by an increase in the degree of synchronization between brain areas, while the former result implies that the interaction strengths between these areas will concurrently get weaker. Although it may appear counter-intuitive that decreased coupling strength would result in increased synchronization, our findings illustrate that these results are not incompatible.

Another important implication of this study follows from our demonstration that systems with simple connection topology are capable of exhibiting very rich dynamical behavior. In particular, many of the patterns seen in our simulations of the network of Macaque brain regions (Fig. 1) resemble those observed using much simpler connectivity schemes (Fig. 3). Hence, patterns seen in complex systems that are often attributed to their non-trivial connection structure, may in fact be independent of the details of the network architecture. In light of recent studies that investigate the collective dynamics of networks reconstructed from real-life data (e.g., Ref. [22]), our results imply that caution should be exercised in linking observed features of a system to specific properties of the underlying network as, in some cases, simpler topologies may reproduce similar patterns. Thus, our findings provide a baseline for future studies on the specific role of the detailed aspects (degree heterogeneity, modular architecture, etc.) of brain networks on their collective dynamics.

To conclude, we have shown that the collective dynamics of a homogeneous system of oscillators, motivated by mesoscopic descriptions of brain activity, exhibits spontaneous symmetry breaking that gives rise to several novel patterns. Despite preserving the structural symmetry

of connections, a marginal increase in the network sparsity, corresponding to an extremely small deviation from the mean-field, unexpectedly changes the robustness of certain patterns. Our results suggest that some of the complicated activity patterns seen in the brain can be explained even without complete knowledge of its wiring diagram.

We thank Raghavendra Singh, Purusattam Ray and Gautam Menon for helpful discussions. We thank IMSc for providing access to the “Annapurna” supercomputer. This research was supported in part by the IMSc Complex Systems Project.

-
- [1] A. Pikovsky, M. Rosenblum, and J. Kurths, *Synchronization* (Cambridge University Press, Cambridge, England, 2003).
- [2] J. A. Acebrón *et al.*, Rev. Mod. Phys. **77**, 137 (2005).
- [3] L. Glass, Nature (London) **410**, 277 (2001); M. U. Gillette and T. J. Sejnowski, Science **309**, 1196 (2005); R. Singh *et al.*, Phys. Rev. Lett. **108**, 068102 (2012).
- [4] A. K. Engel, P. Fries and W. Singer, Nature Rev. Neurosci. **2**, 704 (2001); M. I. Rabinovich, P. Varona, A. I. Selverston and H. D. I. Abarbanel, Rev. Mod. Phys. **78**, 1213 (2006).
- [5] G. Buzsáki and A. Draguhn, Science **304**, 1926 (2004).
- [6] E. R. Kandel, J. H. Schwartz and T. M. Jessell, *Principles of Neural Science* (McGraw-Hill, New York, 4th edition, 2000).
- [7] W. Singer, Ann. Rev. Physiol. **55**, 349 (1993).
- [8] L. D. Lewis *et al.*, Proc. Natl. Acad. Sci. USA **109**, E3377 (2012).
- [9] H. Markram, Nature Rev. Neurosci. **7**, 153 (2006); C. Zhou, L. Zemanová, G. Zamora, C. C. Hilgetag and J. Kurths, Phys. Rev. Lett. **97**, 238103 (2006).
- [10] C. van Vreeswijk and H. Sompolinsky, Science **274**, 1724 (1996).
- [11] G. Deco, V. K. Jirsa, P. A. Robinson, M. Breakspear and K. Friston, PLoS Comput. Biol. **4**, e1000092 (2008).
- [12] J. W. Scannell, C. Blakemore and M. P. Young, J. Neurosci. **15**, 1463 (1995); P. Hagmann, L. Cammoun, X. Gigandet, R. Meuli, C. J. Honey, V. J. Wedeen, and O. Sporns, PLoS Biol. **6**, e159 (2008).
- [13] D. S. Modha and R. Singh, Proc. Natl. Acad. Sci. USA **107**, 13485 (2010).
- [14] G. Palm, Hippocampus **3**, 219 (1993); C. Johansson and A. Lansner, Neural Networks **20**, 48 (2007).
- [15] G. M. Shepherd (Ed.), *The Synaptic Organization of the Brain* (Oxford University Press, New York, 4th edition, 2003); R. Morris, in *The Hippocampus Book* (Eds. P. Andersen *et al.*) (Oxford University Press, Oxford, 2007).
- [16] E. A. Leicht and M. E. J. Newman, Phys. Rev. Lett. **100**, 118703 (2008).
- [17] A. Schnitzler and J. Gross, Nature Rev. Neurosci. **6**, 285 (2005); P. J. Uhlhaas and W. Singer, Nature Rev. Neurosci. **11**, 100 (2010).
- [18] B. H. Jansen and V. G. Rit, Biol. Cybern. **73**, 357 (1995); C. J. Honey, R. Kotter, M. Breakspear and O. Sporns, Proc. Natl. Acad. Sci. USA **104**, 10240 (2007); F. Marten, S. Rodrigues, O. Benjamin, M. P. Richardson and J. R. Terry, Phil. Trans. R. Soc. A **367**, 1145 (2009).
- [19] H. R. Wilson and J. D. Cowan, Biophys. J. **12**, 1 (1972); A. Destexhe and T. J. Sejnowski, Biol. Cybern. **101**, 1 (2009).
- [20] Note that APS, which for $N > 2$ has a very small basin of attraction, is a “phase cluster” state for which $n_{cl} = 2$.
- [21] S. Kar, A. Routray and B. P. Nayak, Clin. Neurophysiol. **122** 966 (2011); C. J. Chu *et al.*, J. Neurosci. **32** 2703 (2012).
- [22] A. Haimovici, E. Tagliazucchi, P. Balenzuela and D. R. Chialvo, Phys. Rev. Lett. **110**, 178101 (2013).

SUPPLEMENTARY MATERIAL

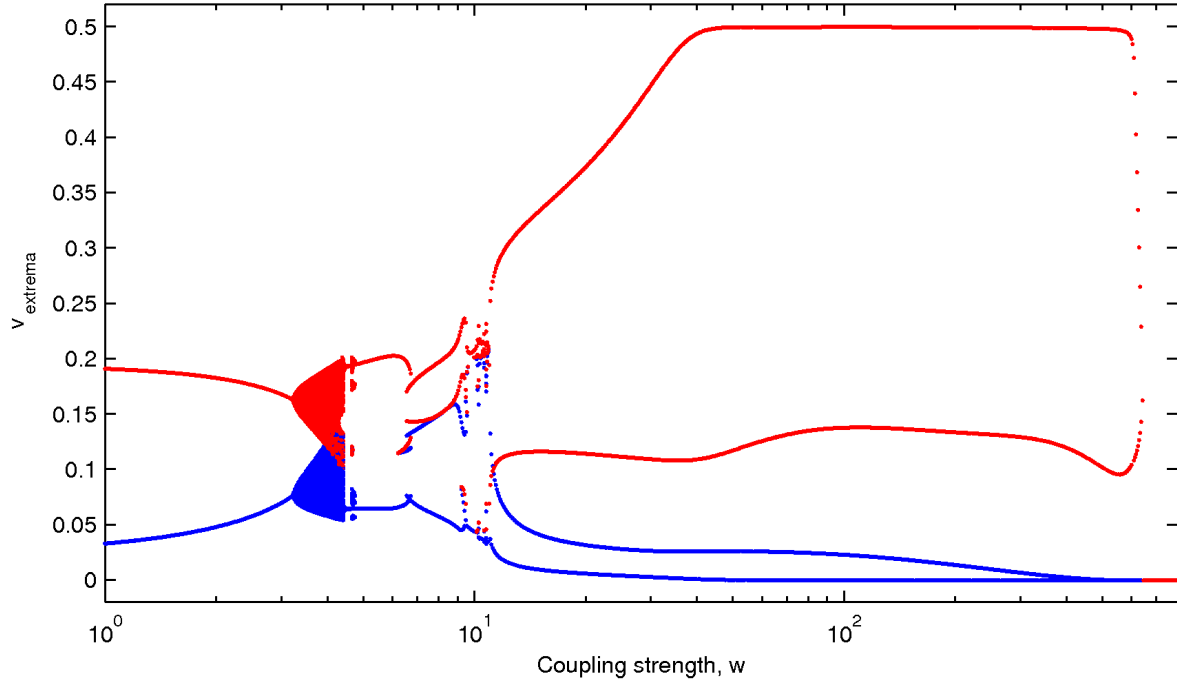


FIG. S1: Bifurcation diagram for a pair of coupled WC oscillators with coupling strength w as the bifurcation parameter, obtained for a set of 20 random initial conditions (i.c.). Red dots represent the maxima of the inhibitory components v for each i.c., while blue dots represent the corresponding minima.

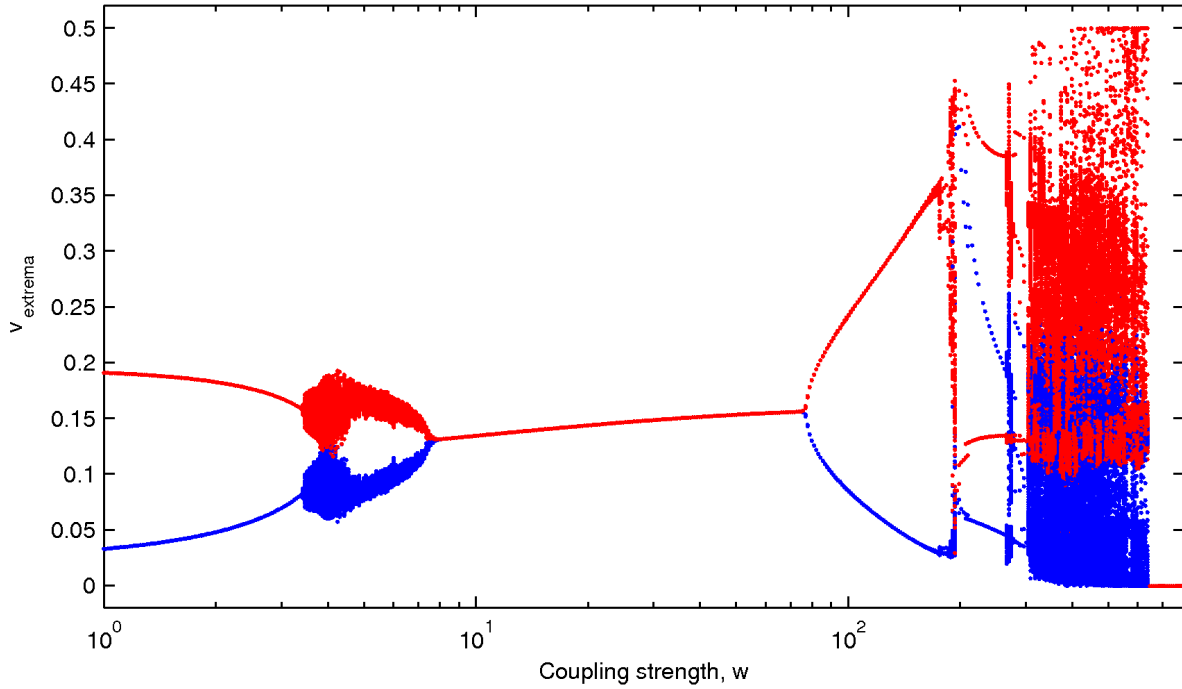


FIG. S2: Bifurcation diagram for $N = 20$ globally coupled WC oscillators with coupling strength w as the bifurcation parameter, obtained for a set of 20 random initial conditions (i.c.). Red dots represent the maxima of the inhibitory components v for each i.c., while blue dots represent the corresponding minima.

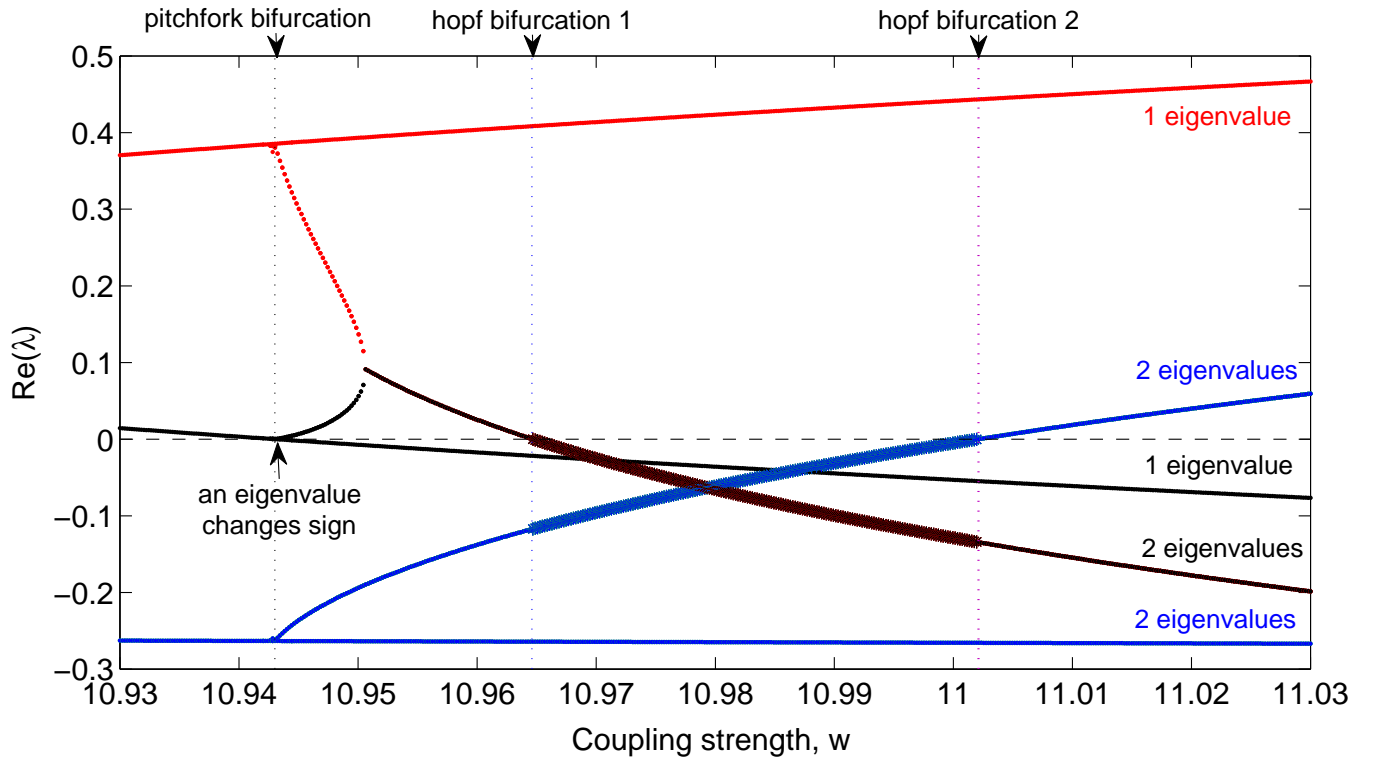


FIG. S3: Real parts of the eigenvalues of all the fixed points for a pair of coupled WC oscillators, shown as a function of coupling strength w in the neighborhood of the transition between APS and IIS regimes. The vertical dotted lines indicate the locations where different bifurcations occur in this range of w . Thick lines between the two Hopf bifurcations represent stable solutions. Three of the branches shown correspond to a pair of eigenvalues, as indicated in the figure.

TABLE S1: Order parameters used for identifying the different dynamical regimes of a homogeneous network of WC oscillators (as explained in the main text).

Pattern	$\langle \sigma_t^2(v_i) \rangle_i = 0$	$\langle \langle v_i \rangle_t \rangle_i = 0$	$\sigma_i^2(\langle v_i \rangle_t) = 0$	$\langle \sigma_i^2(v_i) \rangle_t = 0$	$\Delta > 0$
AD	✓	✓	✓	✓	
OD	✓		✓	✓	
IIS	✓				
ES			✓	✓	
QP					✓
IIS					
GS			✓		